A comprehensive kinetic model for phenol oxidation in seven advanced oxidation processes and considering the effects of halides and carbonate

Kuan Huang and Huichun Zhang*

Department of Civil and Environmental Engineering, Case Western Reserve University, Cleveland, Ohio 44106, United States

Corresponding Author

*Phone: (216) 368-0689; E-mail: hjz13@case.edu.

Abstract

As one of the most powerful approaches to mechanistically understanding complex chemical reaction systems and performing simulations or predictions, kinetic modeling has been widely used to investigate advanced oxidation processes (AOPs). However, most of the available models are built based on limited systems or reaction mechanisms so they cannot be readily extended to other systems or reaction conditions. To overcome such limitations, this study developed a comprehensive model on phenol oxidation with over 550 reactions, covering the most common reaction mechanisms in nine AOPs—four peroxymonosulfate (PMS), four peroxydisulfate (PDS), and one H_2O_2 systems—and considering the effects of co-existing anions (chloride, bromide, and carbonate) and product formation. Existing models in the literature were first gathered and revised by correcting inaccurately used reactions and adding other necessary reactions. Extensive model tuning and validation were then conducted by fitting the model against experimental data from both this study and the literature. When investigating the effects of anions, we found that PDS/CuO suffered the least impact, followed by the H_2O_2/UV and other PDS systems, and finally the PMS

systems. Halogenated organic byproducts were mainly observed in the PMS systems in the presence of halides. Most of the 556 reactions were found to be important based on the sensitivity analysis, with some involving anions even among the most important, which explained why these anions can substantially alter some of the reaction systems. With this comprehensive model, a deep understanding and reliable prediction can be made for the oxidation of phenol (and likely other phenolic compounds) in systems containing one or more of the above AOPs.

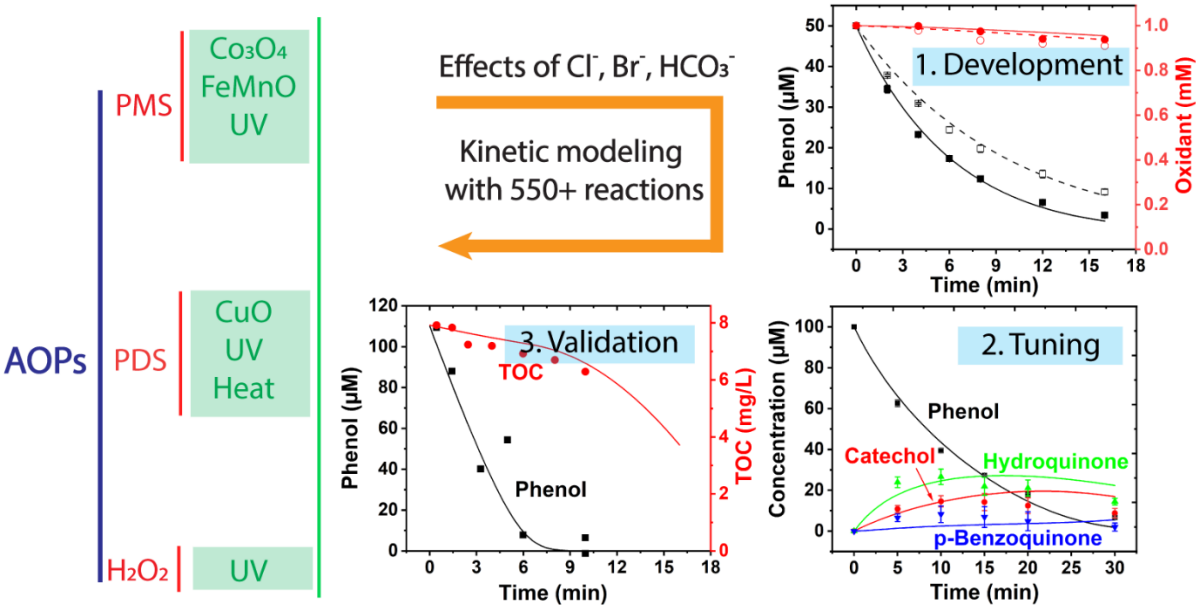

Graphical abstract

Keywords

H_2O_2; Kinetic modeling; Peroxydisulfate; Peroxymonosulfate; Sensitivity analysis; UV irradiation

Highlights

- A comprehensive kinetic model was developed for 7+ AOPs with 550+ reactions;
- Intermediates were considered for the tuning and validation of the model;
- PDS/CuO suffered least from anions followed by H_2O_2/UV and other PDS/PMS systems;

- Sensitivity analysis indicated that anions affected the importance of reactions;
- This model can be easily applied to hybrid systems and different contaminants.

1. Introduction

Advanced oxidation processes (AOPs) are among the most important water treatment technologies for organic contaminant removal. They often rely on the activation of oxidants, such as peroxymonosulfate (PMS), peroxydisulfate (PDS), and H_2O_2, by either energy inputs or catalysts to induce the formation of reactive oxygen species (ROSs), including sulfate ($SO_4^{\bullet-}$) and hydroxyl ($^{\bullet}OH$) radicals (Lee et al., 2020; Wang and Wang, 2018). Recent studies also reported the involvement of singlet oxygen ($^1O_2$) or direct electron transfer (DET) processes in some of the AOP systems (Duan et al., 2018b; Huang and Zhang, 2019). Utilizing the unique long-distance electron transfer property of the prepared catalyst, recent studies developed a "Galvanic oxidation process" that achieved contaminant oxidation even when PMS and the contaminant were physically separated from each other (Huang and Zhang, 2019; 2020a). The reaction mechanisms are usually complex as the reactions between ROSs and organic contaminants generate many intermediates/products. These intermediates/products can further react with the ROSs and their persistence and risks may vary significantly compared to the parent compounds. Moreover, various impact factors exist in real water treatment scenarios, such as the coexisting anions, as mentioned below. They can sometimes significantly alter the reaction mechanisms and impact the contaminant removal efficiency, oxidant utilization efficiency, and product formation.

Kinetic modeling is a powerful approach to gain mechanistic understandings of these systems and can help formulate strategies for improving the treatment efficiency. Extensive modeling studies have been reported for many AOPs, such as H_2O_2/UV, PDS/UV, chlorine/UV,

63 and chloramine/UV (Chuang et al., 2017; Crittenden et al., 1999; Grebel et al., 2010; Yang et al.,
64 2014; 2016). Some best examples include 180 reactions for a H_2O_2/UV system (Grebel et al.,
65 2010), 188 reactions for H_2O_2/UV and PDS/UV systems (Yang et al., 2014), 140 reactions for
66 H_2O_2/UV and PDS/UV systems (Zhang et al., 2015), and 203 reactions for HOCl/UV, H_2O_2/UV,
67 and O_3/UV systems (Bulman et al., 2019). A number of studies have also considered intermediate
68 transformation in their kinetic models (Duesterberg and Waite, 2006; 2007; Guo et al., 2014b;
69 Kang et al., 2002; Li et al., 2004; 2007; Luo et al., 2021; Mora et al., 2011; Qian et al., 2016; Zhao
70 et al., 2021; Zhou et al., 2018). For example, Li et al. performed the kinetic modeling of
71 trichloroethene degradation considering four intermediates and 67 reactions in one system
72 (H_2O_2/UV) (Li et al., 2007). Duesterberg and Waite modeled the oxidation of p-hydroxybenzoic
73 acid with 49 reactions considering one intermediate (3,4-dihydroxybenzoic acid) in the H_2O_2/Fe
74 system (Duesterberg and Waite, 2007). However, a large portion of the reaction rate constants
75 were set as fitting parameters in some studies (e.g., 12 out of 67 (Li et al., 2007), and 13 out of 101
76 (Qian et al., 2016)), which may introduce overparameterization issues. This generally leads to
77 perfect fitting under the studied conditions but potentially poor fitting under other conditions due
78 to the low accuracy of the fitted rate constants. Furthermore, most of these models were built on a
79 limited number of systems and experimental conditions, so they cannot be readily applied to other
80 systems or conditions. As a result, new models need to be developed every time for new systems.
81 This is time consuming and labor intensive. To overcome both the overparameterization issue and
82 applicability limitation, more systems and experimental conditions should be considered to build
83 a robust and comprehensive model.

84 The performance of AOPs is also known to be affected by halides (including Cl^- and Br^-)
85 or carbonate (collectively referred to as the "anions" hereafter), often through generating different

reactive species. For example, Grebel et al. demonstrated that carbonate significantly decreased the phenol degradation rate in a H_2O_2/UV system because the reaction of $^{\bullet}OH$ with carbonate forms less reactive carbonate radicals ($CO_3^{\bullet-}$). Such an effect is much stronger than that of Cl^- but weaker than that of Br^- (Grebel et al., 2010). In PMS-based systems, halides have reportedly accelerated the contaminant removal because of the reactions of PMS with halides to form non-radical RHSs (e.g., HOX, X_2, X = Cl or Br) (Fang et al., 2016; Luo et al., 2019; Wang et al., 2017). These non-radical RHSs can sometimes be very abundant compared to the original ROSs and result in significantly faster contaminant oxidation, although they may also lead to inhibited mineralization and formation of toxic halogenated byproducts (Fang et al., 2016; Luo et al., 2019; Wang et al., 2017). Given the ubiquitous presence of these anions in the aquatic environment, it is important to systematically evaluate their impacts on the performance of different AOPs under various conditions. However, current studies considering anions only focused on very limited numbers of oxidants, activation approaches, and reaction mechanisms in each model. The inclusion of additional oxidants/activation approaches may require a lot more reactions that would otherwise have not been modeled.

To resolve above limitations, a comprehensive model needs to be developed for a large number of systems covering most of the known oxidants and activation mechanisms. It can also be easily applied to, for instance, compare the performance of different systems side by side and simulate the scaled-up water treatment systems under various conditions without having to conduct experimental tests. When hybrid systems are employed in some water treatment scenarios (e.g., PDS and H_2O_2 coupled with UV, catalyst, and heat (Monteagudo et al., 2015)), where multiple reactants and/or activation mechanisms are involved, this comprehensive model would be even more powerful to describe the systems and providing mechanistic understandings.

In this work, four PMS, four PDS, and one H_2O_2 systems were first experimentally evaluated for phenol oxidation in both the absence and presence of anions. Then a comprehensive kinetic model was developed for 7+ AOPs considering different oxidants, activation approaches, reaction mechanisms, and other impact factors. The HOX/UV systems were also included in the model because they existed under some conditions (e.g., the PMS/UV system with Cl^- and Br^- resulting in HOCl/UV and HOBr/UV systems). The intermediate transformation was also modeled. Phenol was selected as the model compound because it is widely used in industries and is toxic to aquatic life (Olmez-Hanci and Arslan-Alaton, 2013). Although it can be relatively easily oxidized by AOPs, phenol is the most basic phenolic compound and shares significant similarity with many other contaminants. Using phenol would be, therefore, helpful to develop a model that can be easily adopted for a wide range of contaminants. Extensive model tuning and validation were then carried out by fitting the model against the experimental data from both this study and the literature. Detailed balancing was performed to fix the reaction loop illegality issues, and the model sensitivity analysis was conducted to evaluate the importance of each reaction. With the developed model, the effect of anions on the reaction mechanisms and the importance of different ROSs responsible for phenol degradation and product formation, were evaluated.

2. Materials and methods

Details in chemicals and materials used in this study can be found in the Supplementary Material (SM) Text S1. The AOP systems were selected to include most of the known reaction mechanisms associated with oxidants PMS, PDS, and H_2O_2; activation approaches; and responsible ROSs. A total of four PMS, four PDS, and one H_2O_2 systems were investigated (details in Text S2). Detailed experimental procedures and analytical methods can be found in Text S3,

132 including the UV intensity and pathlength determination, catalyst preparation, experimental setup,
133 and the quantification of PMS, PDS, H_2O_2, phenol, and the degradation products.

134 2.1. Kinetic modeling

135 The model development consisted of four stages, i.e., initial development, improvement,
136 tuning, and validation. We first conducted an extensive literature review and compiled all reported
137 reactions that may occur in the studied systems. Most of the rate constants were obtained from the
138 literature. 40 of them were estimated (e.g., based on the linear correlations between the natural log
139 of the second-order rate constant k ($ln\ k$) and the reduction potentials of the oxidants (Grebel et al.,
140 2010; Pavitt et al., 2017; Zagal et al., 2019), details in Fig. S1 and Table S4 (with 95% confidence
141 intervals)). 8 were obtained by setting them as the fitting parameters while fitting the model against
142 the experimental data. For reactions that were inaccurately applied in the literature, revisions were
143 also made (details in Section 3.3). The whole model was built using the computer program
144 Kintecus 6.8 (Ianni). To include the effects of ionic strength and temperature on the reaction rate
145 constants, the Davies Equation and the Van't Hoff rules were applied, respectively (details in Text
146 S4).

147 For the UV-based systems, the photolysis rate of the oxidants for the formation of radicals
148 may change considerably throughout the reaction due to the change of the chemical compositions.
149 More details about how to dynamically calculate the photolysis rate in Kintecus for a given system
150 can be found in Text S5.

151 The stages 1-4 of model development can be found in Text S6.

152

153 2.2. Detailed balancing using DETBAL

154 Kinetic models in AOPs can consist of hundreds of reactions; many of these reactions form
155 loops which sometimes violate the principles of detailed balancing (Stanbury, 2020; Stanbury and

156 Harshman, 2019). Two types of violations are commonly encountered (Fig. 1): (1) unopposed
157 irreversible reactions making the loop illegal, and (2) the rate constants of the reactions in a legal
158 loop do not meet the equilibrium requirement (Wegscheider's condition). A computer program
159 called "DETBAL" has been developed recently (Stanbury, 2020; Stanbury and Harshman, 2019)
160 and was used in this study to solve these violations. More details about the principles and the
161 program can be found in Text S7.
162

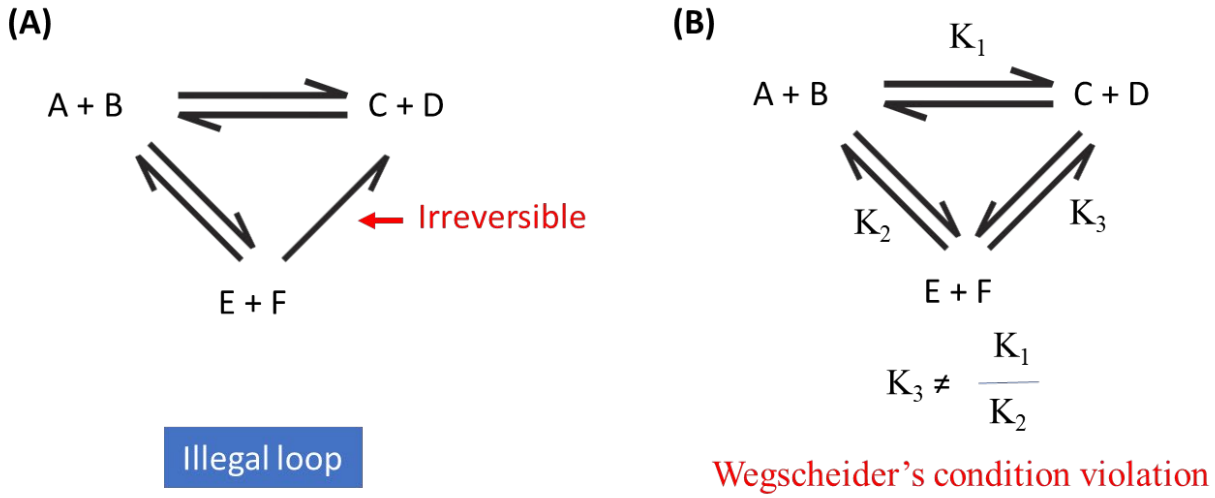

163
164
165 **Fig. 1.** Two types of detailed balancing violations: (A) illegal loops, and (B) violation of the
166 Wegscheider's condition.
167
168 2.3. Model overparameterization control
169 Setting a reasonable number of fitting parameters can be helpful to obtain values that are
170 difficult to be directly measured. However, this may lead to over-parameterization—perfect
171 fittings under the studied conditions, but poor fittings under other conditions due to the low
172 accuracy of the fitted rate constants. This is more likely when the number of fitting parameters is

larger than that of the fitted datasets. Keeping the number of fitting parameters smaller than that of the experimental conditions is an effective way to avoid this issue.

2.4. Model sensitivity analysis

As this model consists of a large number of reactions and it is unclear whether or not all of them are important for the model, sensitivity analysis must be performed. To do that, we used the built-in function in Kintecus to calculate the normalized sensitivity coefficients (NSCs) with the command "*-SENSIT:1:3*" (see the Kintecus manual for details). The NSCs are the normalized partial derivatives of each species with respect to each reaction rate constant (Eq. A). In other words, Kintecus changes the rate constant k of a specific reaction and determines how the concentrations of all the species in the reaction system respond to this change—the number of the calculated NSCs is therefore equal to that of the total species. When the responses are significant (large absolute NSCs) for some species, this reaction is important, and *vice versa*. Following this method, Kintecus changes all the k values one by one and see how the concentrations of all the species in the system are affected. As a result, this process provides a 2D vector (matrix) with the number of NSCs equal to the number of reactions multiplied by the number of species, as shown in the Excel file "Huang and Zhang_Kinetic modeling.xlsx" in the Supplementary Material.

$$NSC = \left(\frac{\frac{\partial[Speices]}{[Species]}}{\frac{\partial k}{k}}\right)_k = \left(\frac{\partial ln[Speices]}{\partial lnk}\right)_k \quad \text{(A)}$$

3. Results and discussion

3.1. Performance of the nine AOP systems

The phenol degradation rates and oxidant utilization efficiencies were evaluated in the absence and presence of the anions (including Cl^-, Br^- and HCO_3^-), as shown in Fig. 2. In the three

UV systems without the anions, PDS showed the highest phenol degradation rate followed by H_2O_2 and then PMS, while this order changed to PDS > PMS > H_2O_2 in the presence of the anions. The orders of the oxidant utilization efficiencies were H_2O_2 > PDS > PMS and PMS > PDS > H_2O_2 under the UV condition with and without anions, respectively. These were mainly due to the different photoproperties of these oxidants and the reaction rate constants of phenol/intermediates with different ROSs. Additional discussion can be found in Text S8.

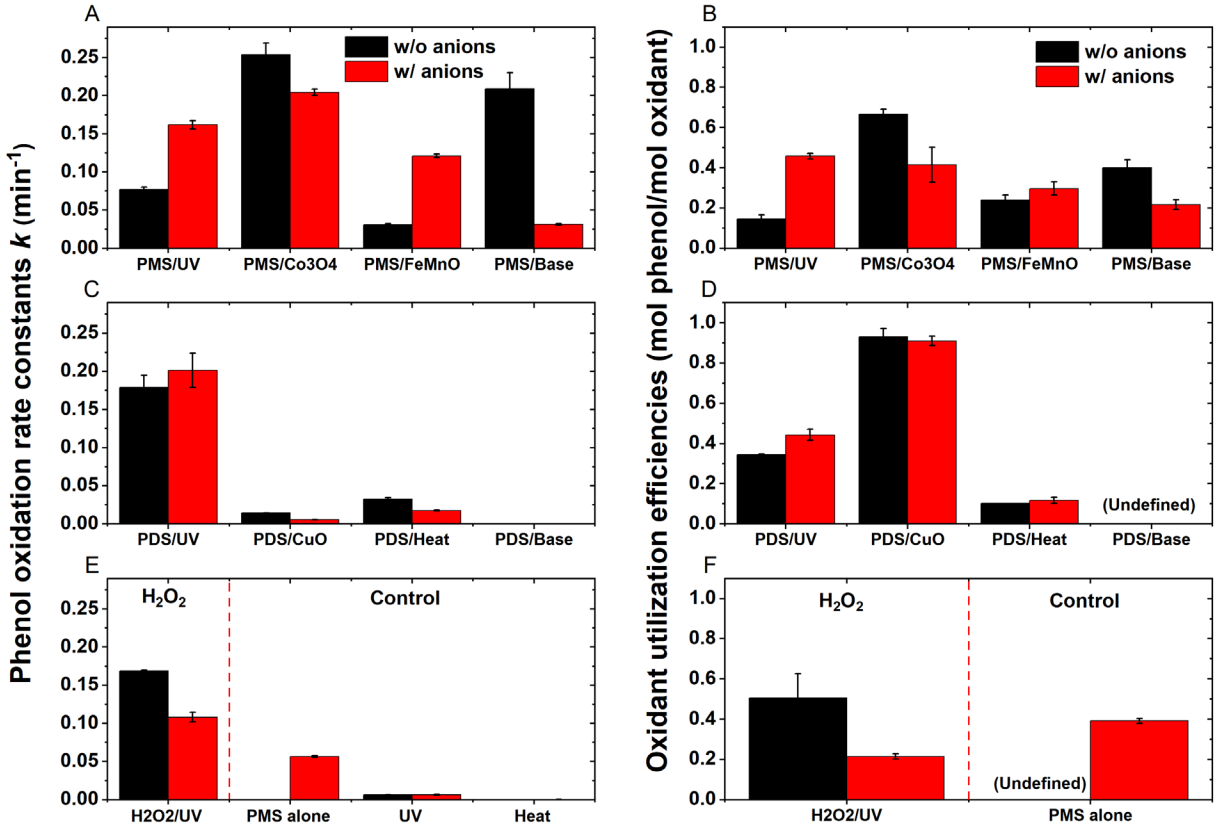

Fig. 2. Left: Pseudo first order phenol degradation rate constants in (A) PMS, (C) PDS, (E) H_2O_2 and the corresponding control systems; Right: oxidant utilization efficiencies of (B) PMS, (D) PDS, (F) H_2O_2 and the corresponding control systems. No bars on the left panel indicate no appreciable phenol transformation detected. The oxidant utilization efficiencies are "undefined" in some systems (D and F) because the oxidant consumption (denominator) is zero. Experimental conditions: $[oxidant]_0$ = 1 mM, $[phenol]_0$ = 50 μM, pH = 7 with 20 mM of borate buffer for all but

the base systems. The activation conditions included UV at 254 nm (for UV systems), heat at 70 °C (for PDS/heat system), base at pH 10 with 20 mM of borate buffer (for base systems), or catalyst at 0.1 g/L (for catalyst systems). "w/ anions" indicated $[Cl^-]_0$ = 141 mM, $[Br^-]_0$ = 0.05 mM, and $[HCO_3^-]_0$ = 11.5 mM. Error bars represent the data range of experimental replicates (n ⩾ 2).

3.2. Initial model development (stage 1)

This stage of model development mainly involves the initiation reactions (Table S3) and the transformation of ROSs. Overall, the fitting was poor for most of the systems. For example, for the PMS/UV and PDS/UV systems, the phenol degradation rates seemed to be constant as the reactions went on, being underestimated at the beginning but overestimated at the end of the reactions (Fig. S2). This is potentially because some important reactions and intermediate transformations were not yet considered. In reality, intermediates may compete with the parent compound for the consumption of ROSs to decrease the phenol degradation rate as the reaction continues. Therefore, considering more reactions as well as the formation of intermediates/products may significantly improve the model. Nevertheless, at the current stage, we also observed that, according to the primary ROS transformation pathways in the presence of halides (Scheme S1), some of the species such as $Cl_2^{\bullet-}$, $Br_2^{\bullet-}$, $Cl^{\bullet}$, and $HO_2^{\bullet}$ served as important bridges for the transformation of other species. Some of them such as $Cl_2^{\bullet-}$ and $Br_2^{\bullet-}$ were indeed later found to be important contributors to the contaminant oxidation (Section 3.6).

3.3. Model improvement (stage 2)

In the process of model development, we observed that some reactions have been inaccurately used in some of the previous modeling studies. For example, O_2 was often treated as

the product in the $^{\bullet}OH + HO_2^{\bullet}/O_2^{\bullet-}$ type of reactions (Reactions 100-103, Table S1) (Cheng et al., 2018; Crittenden et al., 1999; Grebel et al., 2010; Yang et al., 2014). However, recent studies have performed convincing experiments, such as the enhancing and quenching tests on a chemiluminescence system, electron spin resonance, and chemical trapping by mass spectrometry, to demonstrate the formation of $^1O_2$ rather than O_2 (Li et al., 2015; Lin and Liu, 2008; Liu et al., 2006; Qi et al., 2016; Zhou et al., 2013). Therefore, we adopted $^1O_2$ as the product here. The $^{\bullet}OH + HO_2^{\bullet}/O_2^{\bullet-}$ type of reactions are also the primary steps in the formation of $^1O_2$ in base-activated PMS (Duan et al., 2018b; Qi et al., 2016). Similarly, the reactions of radical RHSs with $HO_2^{\bullet}$ or $O_2^{\bullet-}$, including Reactions 56, 57, 78, 79, 119, 137, and 138 in Table S1, should also form $^1O_2$ instead of O_2 because these RHSs can be easily converted from and to $^{\bullet}OH$. In addition, the oxygen as a product in the reactions of H_2O_2 with HOX/X_2 has been reported to be all at the excited state ($^1O_2$), as shown in Reactions 108, 111, 112, 123, 128, 129, 130, and 134 in Table S1 (Held et al., 1978; Khan and Kasha, 1970; Piatt and O'brien, 1979), but many modeling studies adopted O_2 rather than $^1O_2$ (Bulman et al., 2019; Cheng et al., 2018; Grebel et al., 2010; Yang et al., 2014; Zhang et al., 2015). More discussions can be found in Text S9.

Studies have also frequently neglected the important roles of $S_2O_8^{\bullet-}$ and $ClO^{\bullet}$. As they have been proven to be strong oxidants and can effectively oxidize a wide range of organic contaminants (Alfassi et al., 1988; Bulman et al., 2019; Duan et al., 2018a; Kong et al., 2018; Wu et al., 2016), they were included in the model. More details can be found in Text S9.

Upon the incorporation of the above reactions, the improved model was fitted against the experimental data, as shown in Figs. 3A-G. By making the four unavailable rate constants as the fitting parameters (Reactions 1, 3, 5, and 6 in Table S1), we were able to obtain good fittings for all the seven systems with and without the anions (14 systems in total). This suggested that the

model can describe the systems well. Another indication of the good model performance is that the model-fitted rate constant of PDS activation by heat was 7.8×10^{-6} s^{-1}, close to the reported value of 5.4×10^{-6} s^{-1} under similar conditions (70 °C, pH 5) (Yang et al., 2019).

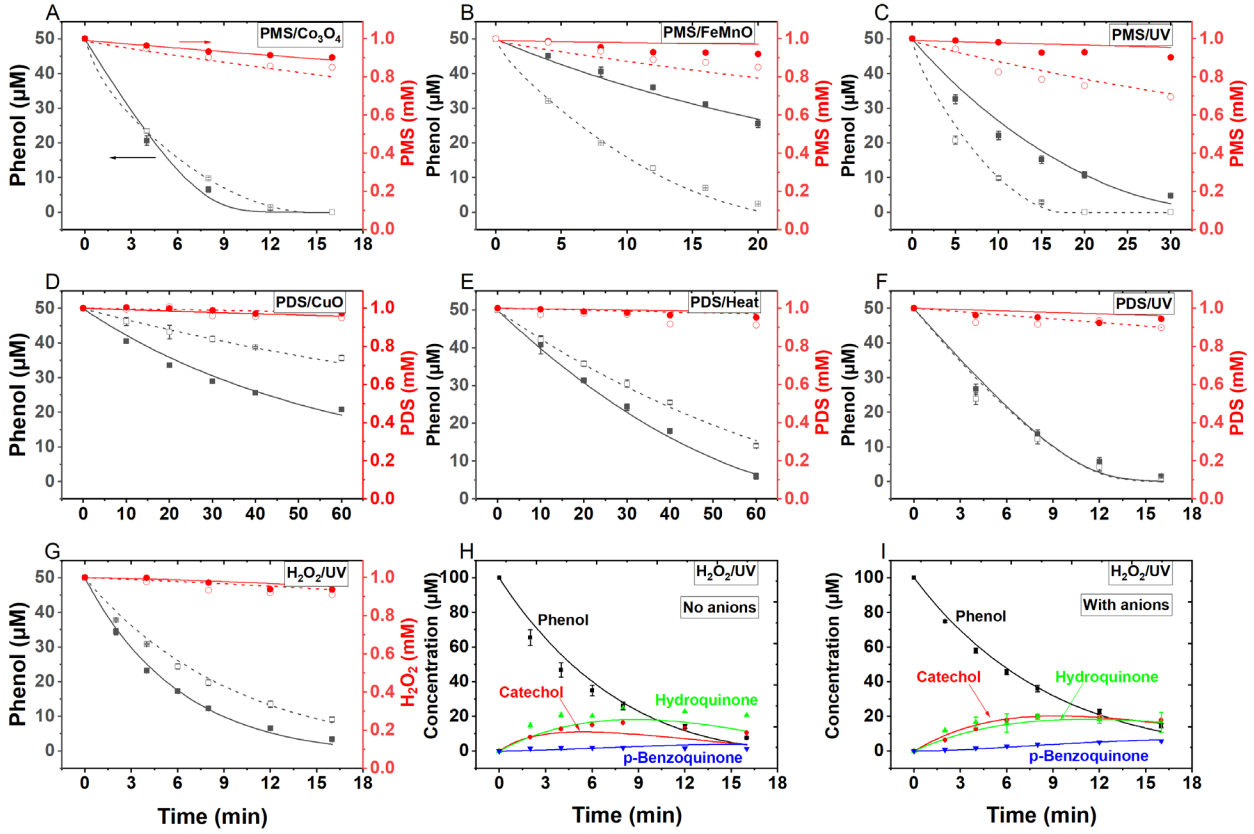

Fig. 3. (A-G) Stage 2 model improvement by fitting against the experimental phenol degradation (black) and oxidant consumption (red) data of the systems PMS/Co_3O_4, PMS/FeMnO, PMS/UV, PDS/CuO, PDS/heat, PDS/UV, and H_2O_2/UV with or without the anions. The solid and open points are the experimental data in the absence and presence of the anions, respectively. The solid and dashed lines are the model simulation results. Experimental conditions: $[oxidant]_0$ = 1 mM, $[phenol]_0$ = 50 μM, pH = 7 with 20 mM borate buffer, and 70 °C for PDS/heat systems. (H-I) Model tuning by fitting against the experimental data of the systems H_2O_2/UV with and without the anions under the conditions: $[H_2O_2]_0$ = 2 mM, $[phenol]_0$ = 100 μM, pH = 7 with 20 mM borate

buffer. The simulation of a few intermediates that were not experimentally monitored are illustrated in Fig. S4. Error bars represent the data ranges of experimental replicates (n ⩾ 2).

3.4. Model tuning (stage 3)

3.4.1. Inclusion of degradation intermediates

Although the model developed in stage 2 showed satisfactory fitting results for both phenol and the oxidants, the formation and further transformation of intermediates/products were still not included.

Overall, the oxidation of phenol by radical and non-radical species goes through two pathways, as illustrated in Schemes 1 A and B, respectively. More details can be found in Text S10 and Scheme S2.

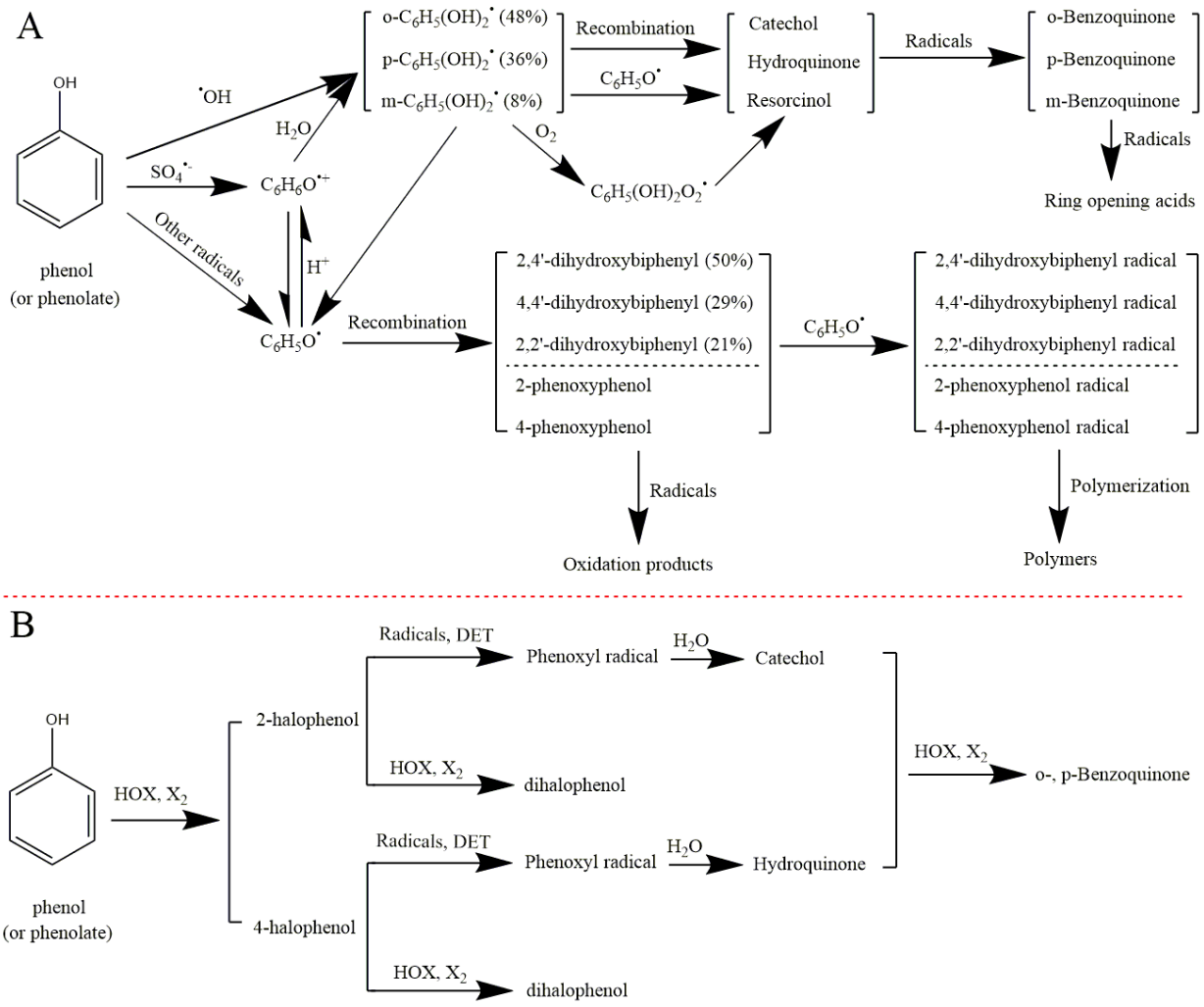

Scheme 1. Pathways of phenol transformation by (A) radical ROSs and (B) non-radical RHSs.

After incorporating the above pathways into the model, we conducted another series of experiments with a higher initial phenol concentration for the systems of PMS/Co_3O_4, PDS/UV, and H_2O_2/UV with or without the anions. As it is challenging to model all possible intermediates in AOPs even for simple compounds (Kamath et al., 2018), we only monitored some of the most important ones, including catechol, hydroquinone, and p-benzoquinone. The model was then fit against the experimental data. As shown in Figs. 3H-I and S3, by making four additional unknown rate constants as the fitting parameters (Reactions 285, 375, 376, and 490 in Table S1), we observed good fittings for all the 6 systems. This suggested that this comprehensive model can

289 simulate the product transformation well. The details of the finalized model containing a total of
290 556 reactions can be found in Table S1.
291
292 *3.4.2. Detailed balancing using DETBAL*
293 The first round of detailed balancing analysis identified a total of 315 loops and two of
294 them were illegal. The fundamental elements of these loops were all reactions. The second round
295 of analysis was performed by checking whether these small loops can form larger loops. As a
296 result, a total of 24 illegal loops were further identified, each containing small loops as the elements.
297 In addition, a total of 16 loops were found to disagree with the Wegscheider's condition. These
298 issues were fixed following the approaches described in Section 2.2 and Text S7. Because such a
299 detailed balancing process has not been widely adopted in the literature, it would be helpful to
300 keep but mark the reactions that were removed to illustrate the modifications, as shown in Table
301 S1 (26 crossed and highlighted reactions). Overall, the removal of these reactions did not lead to
302 significant changes in the species we monitored during the simulation, especially when anions
303 were not present (data not shown).
304
305 *3.4.3. Model overparameterization control*
306 In this study, a total of 8 fitting parameters were used while more than 20 experimental
307 conditions (different oxidants, activation approaches, presence or absence of anions, and reactant
308 concentrations) were fitted. Therefore, overparameterization was largely avoided.
309

3.5. Model validation (stage 4)

After the development of the model, a third batch of experiments was carried out for four systems, i.e., PMS/UV and PDS/heat with and without the anions, to validate the model. As shown in Figs. 4A-C and S5A, the model demonstrated very good simulation for phenol and the three intermediates in all the four systems. The difference in the intermediate formation was mainly due to the significant alteration of the major ROSs responsible for phenol oxidation (Tables S6 and S7), which resulted in different pathways of intermediate formation (Scheme 1). The effects of anions are discussed in Section 3.6.

In addition to the experimental data collected in this study, the kinetic results for a few external systems were extracted from the literature for model validation. For example, a H_2O_2/UV system was selected under the experimental conditions of $[phenol]_0$ = 5.17 mM, $[H_2O_2]_0$ = 0.245 M, and temperature = 45 °C (Alnaizy and Akgerman, 2000). The UV irradiation parameters were slightly adjusted to reflect the different UV intensity, effective path length and possible UV length. As shown in Fig. 4D, the model fitted moderately well to the degradation of phenol and the evolution of catechol and hydroquinone. We believe these fits are reasonable given that some of the reaction conditions were unknown, such as the ionic strength and potential introduction of halides during the solution preparation. Based on the kinetic data from another study (Mora et al., 2011), the phenol and TOC (total organic carbon) removal was modeled for a PDS/heat system under three conditions, as shown in Figs. 4E-F and S5B. The TOC was calculated by the sum of the carbon weights from the major organic compounds, including phenol, o-, p-, and m-benzoquinones, and dihydroxybenzenes. Other species such as dihydroxybiphenyls and phenoxyphenols were also included but they did not make noticeable contributions (See the Excel file "Huang and Zhang_Kinetic modeling.xlsx" in the Supplementary Material for details).

Surprisingly, the model demonstrated good fits to the phenol and TOC trends although TOC was never used during the model development. This further validated the obtained model.

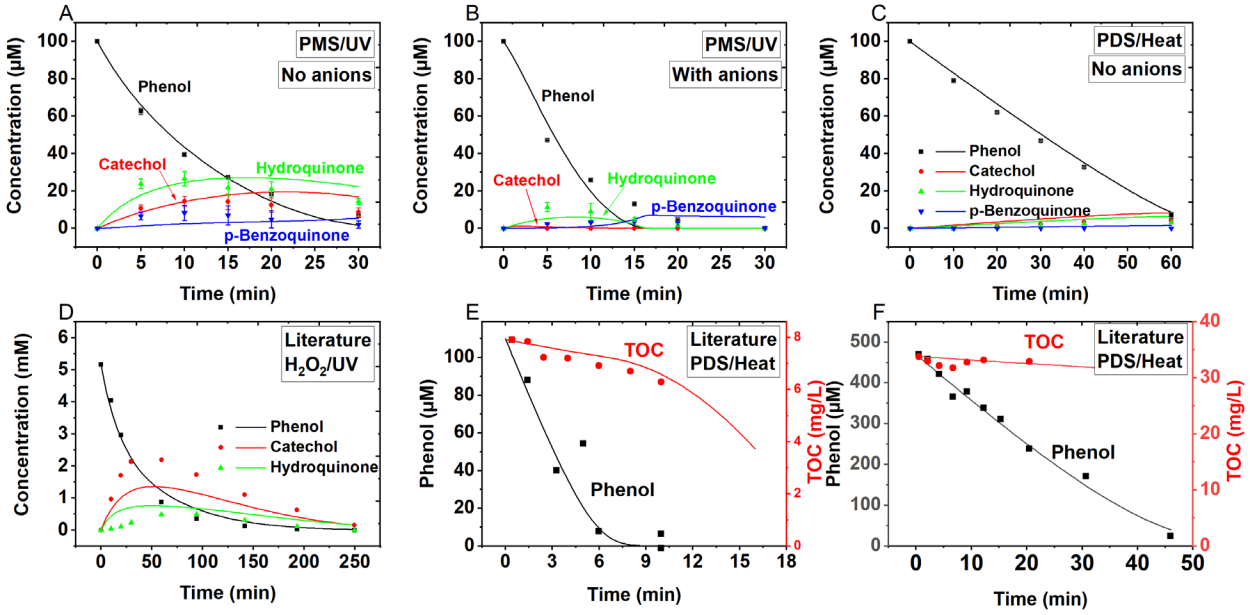

Fig. 4. First row: Model validation by fitting against the experimental data of systems (A) PMS/UV without the anions and (B) PMS/UV with the anions, both under the conditions: $[PMS]_0$ = 2 mM, $[phenol]_0$ = 100 μM, pH = 7 with 20 mM borate buffer; and (C) PDS/heat without the anions under conditions: $[PDS]_0$ = 2 mM, $[phenol]_0$ = 100 μM, pH = 7 with 20 mM borate buffer, and 70 °C. Error bars represent the data ranges of experimental replicates (n ⩾ 2). Second row: Model validation by fitting against the data from the literature of systems (D) H_2O_2/UV under conditions: $[phenol]_0$ = 5.17 mM, $[H_2O_2]_0$ = 0.245 M, and 45 °C (Alnaizy and Akgerman, 2000); (E) PDS/heat under conditions: $[PDS]_0$ = 10 mM, $[phenol]_0$ = 110 μM, $[TOC]_0$ = 7.4 mg/L, pH = 2, and 70 °C (Mora et al., 2011); and (F) PDS/heat under conditions: $[PDS]_0$ = 10 mM, $[phenol]_0$ = 470 μM, $[TOC]_0$ = 31.8 mg/L, pH = 2, and 70 °C (Mora et al., 2011).

3.6. Effects of the anions and contributions of different ROSs

With the developed model, the phenol degradation kinetics and the contribution of different ROSs can be easily simulated under different reaction conditions. We tried different combinations of Cl^-, Br^-, and HCO_3^- to examine how the systems responded to the changes. As shown in Tables S6 and S7, in the absence of the anions, the phenol degradation in all the systems is almost always attributed to well-known ROSs or pathways (This result was obtained by simply tracking the phenol reactions with other species in the Kintecus program (details in Text S11)). For example, in Table S6, $SO_4^{\bullet-}$ contributed to 99.8% of phenol degradation in the PMS/Co_3O_4 system, and DET was responsible for 100% in the PMS/FeMnO system. However, in the presence of the three anions, the largest contributors in the PMS/Co_3O_4 system shifted to $CO_3^{\bullet-}$ (72.2%) and HOBr (11.5%), while $SO_4^{\bullet-}$ only contributed 4.6%. A similar phenomenon existed in all other PMS systems. In addition to the reactions of the anions with the radicals, Cl^- and Br^- can also react with PMS at relatively high rates (k = 1.8 × 10^{-3} and 0.7 M^{-1} s^{-1}, respectively) to form HOX and subsequently other non-radical RHSs (Huang and Zhang, 2020b). These species could be abundant and contributed to the fast phenol oxidation, as shown in Fig. 2. Therefore, the PMS systems can be more susceptible to the matrix effects than the PDS or H_2O_2 systems. For the PDS systems (Table S7), DET, $SO_4^{\bullet-}$, and $SO_4^{\bullet-}$ contributed to around 100% of phenol degradation in PDS/CuO, PDS/Heat, and PDS/UV systems, respectively, in the absence of the anions. In the presence of the three anions, however, the key species were found to be $S_2O_8^{\bullet-}$ in both PDS/Heat and PDS/UV systems. None of the three anions affected the PDS/CuO system. As mentioned earlier, the PDS/CuO system under neutral conditions solely relies on DET for phenol oxidation. Therefore, although Cl^-, Br^-, and HCO_3^- may inhibit this process by affecting the complexation between PDS and CuO, no new ROSs would generate to a noticeable level to alter the reaction mechanism.

For the H_2O_2/UV system, $^{\bullet}OH$ contributed to more than 80% of the phenol degradation under all the conditions. This indicates that H_2O_2/UV has higher robustness than the PDS/UV and PDS/heat systems. This agrees well with a study reporting that Cl^- did not exhibit noticeable effects on the 2,4,6-trichlorophenol oxidation and product formation in a H_2O_2/UV system (Fang et al., 2016). This might be due to the milder scavenging effects of the anions on $^{\bullet}OH$ than on $SO_4^{\bullet-}$. As shown in Eqs. B and C, X^- generally reacts with $^{\bullet}OH$ to form $HOX^{\bullet-}$, which proceeds to form OH^- and $X^{\bullet}$. In contrast, X^- often reacts with $SO_4^{\bullet-}$ to directly form SO_4^{2-} and $X^{\bullet}$. According to the rate constants of Reactions 37-42, 62-64, 66, and 67 (Table S1), such a scavenging effect is much more pronounced on $SO_4^{\bullet-}$ than on $^{\bullet}OH$. This has also been reported in another study (Zhang and Parker, 2018). Therefore, following the PDS/CuO system, H_2O_2/UV would be the second most robust system regarding the effect of halides.

$$^{\bullet}OH + X^- \rightleftharpoons HOX^{\bullet-} \rightleftharpoons OH^- + X^{\bullet} \quad (B)$$

$$SO_4^{\bullet-} + X^- \rightleftharpoons SO_4^{2-} + X^{\bullet} \quad (C)$$

3.7. Prediction of intermediate formation

Another advantage of having a comprehensive model is to easily predict the intermediate formation under different conditions without having to carry out any experiments. The simulated product formation for different systems and conditions are shown in Tables S8 and S9. HCO_3^- slightly altered the product distribution but did not change the types of products for all the systems. Upon the addition of Cl^- and/or Br^-, however, significant amounts of halogenated products such as halophenols, dihalophenols, and haloresorcinols formed in all the PMS-based systems. As mentioned above, this shift was primarily due to the formed non-radical RHSs resulting in the halide-substitution reactions. In contrast, halides did not exhibit such an effect in any of the PDS

or H_2O_2 systems because of the negligible formation of non-radical RHSs. On the other hand, although halides can result in radical RHSs in some of the systems, as mentioned above, these RHSs generally oxidize organic compounds through electron transfer reactions rather than halide substitution (Grebel et al., 2010). This agrees well with another study reporting that only 0.03% of halophenols formed in a H_2O_2/UV system with a halide level similar to that in this study (Grebel et al., 2010). Therefore, we conclude that the formation of halogenated byproducts would primarily be a concern for the PMS-based systems but not for the PDS or H_2O_2 systems, especially when the halide concentrations are low and the reaction time is short (e.g., less than 60 min). Although not modeled, the system of PMS/base may not form halogenated byproducts either because the reactions between PMS and halides can be significantly retarded under alkaline conditions (Huang and Zhang, 2020b).

3.8. Model sensitivity analysis

To identify the most important reactions in all the AOP systems (assuming merging the seven systems into one), we performed sensitivity analysis in the presence of anions by including all the initiation reactions in Table S3. As shown in the Excel file "Huang and Zhang_Kinetic modeling.xlsx" in the Supplementary Material and Fig. S6, the sensitivity analysis was conducted for the beginning (1 s), the middle (480 s), and the end (960 s) of the reactions based on the model simulations. However, since some of the reactions have not started at the beginning while others have already completed at the end, the sensitivity analyses for the systems at these times may not accurately reflect the real importance of these reactions. Therefore, hereafter we mainly interpret the results at the middle of the simulated reactions (480 s). Positive NSCs indicate positive contributions of the corresponding reactions to the corresponding species while negative results

suggest negative contributions. Larger absolute values generally mean higher importance of the reactions. As different reactions contribute differently to different species, and the species of interest usually change from case to case, we decided to sum all the positive, negative, and absolute NSC values for each reaction to show their overall importance to the whole system, as shown in the sheet "Sensitivity_480s, columns 'DP, DQ, and DR'" in the Excel file.

A total of 26 reactions (with green color) was found to have no or minimum contributions to all the species. Most of these reactions involve uncommon species such as BrO_2^-, $BrOCl{\bullet}H_2O$, and $BrClO_2$. On the other hand, it is interesting to know that overall, the reaction $CO_3^{\bullet-} + H_2O_2 \rightarrow HCO_3^- + HO_2^{\bullet}$ (Reaction 144) was the most important (but negatively). $CO_3^{\bullet-} + S_2O_8^{2-} \rightarrow CO_3^{2-} + S_2O_8^{\bullet-}$ (Reaction 149) had the largest positive contribution followed by $Br^- + HSO_5^- \rightarrow HOBr + SO_4^{2-}$ (Reaction 165). This might be because the formed $S_2O_8^{\bullet-}$ and HOBr are strong oxidants and can oxidize a wide range of organics or facilitate other reactions. More details about the importance of each reaction can be found in the Excel file. By using the filters in the spreadsheet, one can check which reaction is most important for a specific species. Overall, all the top reactions are those we are already familiar with, and many of them have been included in Scheme S1. It is also interesting to know that many reactions (especially those related to the anions) are more important than the initiation reactions in Table S3. This explains why the presence of anions in some cases can significantly alter the reaction pathways and the product formation. With this sensitivity analysis approach, one can also easily analyze the importance of reactions to understand why and how different reaction conditions affect the whole system.

3.9. Model applicability to other reaction systems or contaminants

Although the development of this model only involved seven systems, it covers most of the known reaction mechanisms in AOPs with PMS, PDS, or H_2O_2 as the oxidant, including radical, non-radical, and DET processes. Therefore, this model can be easily applied to many other systems (e.g., hybrid systems) with only minor modifications, mostly by adding necessary initiation reactions. For example, in a study where PDS and H_2O_2 were activated simultaneously by UV, catalyst, and heat (Monteagudo et al., 2015), existing models would not be able to provide mechanistic insights for the system. However, the model developed in this study can easily do so. For other AOPs pertaining to different oxidants such as ozone (e.g., O_3, O_3/UV, O_3/H_2O_2, and O_3/PMS), these systems generally form $^{\bullet}OH$ and/or $SO_4^{\bullet-}$ as the primary ROSs and, thus, can be well simulated using the current model as well.

This new model is also significant in that, although only phenol was used as the parent contaminant, it can be easily extended to many other contaminants. This is because nearly half of the reactions are about the ROS transformation and can be directly reused, while many of the remaining reactions can be adopted if the contaminants or reaction intermediates contain compounds such as monohalophenols, dihalophenols, dihydroxybenzenes, and benzoquinones. Moreover, recent studies developed a computer program based on known reaction rules to automatically generate the reaction pathways of a given organic contaminant with $^{\bullet}OH$ (Guo et al., 2014a; Guo et al., 2014b). The reaction rate constants of the intermediates/products with $^{\bullet}OH$ can be predicted using reported quantitative structure-activity relationship (QSAR) models (Zhong et al., 2020a; Zhong et al., 2020b). Such QSAR models are under rapid development for different ROSs thanks to the application of machine learning (Zhong et al., 2020a; Zhong et al., 2020b). The current limitation is that the computer program is still limited to $^{\bullet}OH$. If it can be further

461 improved to generate reaction pathways for other ROSs, it would be promising to couple it with
462 the model developed in this study to substantially expand the applicability of both tools.
463
464 **4. Conclusion**
465 This study first evaluated the performance (phenol degradation rates and oxidant utilization
466 efficiencies) of four PMS, four PDS, and one H_2O_2 systems for phenol oxidation in the absence or
467 presence of halides and carbonate. A comprehensive kinetic model was then built based on seven
468 systems with over 550 reactions. Compared to previous modeling studies, this work considerably
469 improved the model by combining all possible reactions and revising the reactions that have been
470 inaccurately applied in other models. The transformation of a number of intermediates/products
471 was considered to gain a more detailed understanding of the systems. The application of various
472 modeling approaches, from detailed balancing using DETBAL, to overparameterization control,
473 and to model validation with additional measurements and external systems, also significantly
474 improved the reliability of the obtained model. Different from most other kinetic models, each of
475 which was built for mostly single systems, the model developed in this study can be applied to
476 complex hybrid systems involving different oxidants and/or activation mechanisms. Our modeling
477 results revealed that, among the 7 AOPs, the PDS/CuO system was the most robust against the
478 impact of halides and carbonate, followed by the H_2O_2/UV system, and the rest of PDS and PMS
479 systems.
480 However, this model also has a few limitations. For example, the number of the
481 experimentally measured intermediates is small, which indicates that the prediction of other
482 intermediates may not be as reliable as them. In addition, only three co-existing ions are considered
483 in this study. In reality, many other ions and organics (e.g., NOM) may also be present in the target

484 water. Their roles in the kinetic model and effects on the water treatment should be investigated
485 as well.
486
487 **Declaration of competing interest**
488 The authors declare that they have no known competing financial interests or personal
489 relationships that could have appeared to influence the work reported in this paper.
490
491 **Acknowledgments**
492 This work was funded by the National Science Foundation Grant CHE-1808406.
493
494 **Appendix A. Supplementary data**
495 Supplementary data to this article can be found online.
496
497 **References**
498 Alfassi, Z.B., Huie, R.E., Mosseri, S., Neta, P., 1988. Kinetics of one-electron oxidation by the
499 ClO radical. Radiat. Phys. Chem. 32 (1), 85-88.
500 Alnaizy, R., Akgerman, A., 2000. Advanced oxidation of phenolic compounds. Adv. Environ. Res.
501 4 (3), 233-244.
502 Bulman, D.M., Mezyk, S.P., Remucal, C.K., 2019. The impact of pH and irradiation wavelength
503 on the production of reactive oxidants during chlorine photolysis. Environ. Sci. Technol. 53 (8),
504 4450-4459.

505 Cheng, S., Zhang, X., Yang, X., Shang, C., Song, W., Fang, J., Pan, Y., 2018. The multiple role
506 of bromide ion in PPCPs degradation under UV/Chlorine treatment. Environ. Sci. Technol. 52 (4),
507 1806-1816.
508 Chuang, Y.H., Chen, S., Chinn, C.J., Mitch, W.A., 2017. Comparing the UV/Monochloramine and
509 UV/Free chlorine advanced oxidation processes (AOPs) to the UV/Hydrogen peroxide AOP under
510 scenarios relevant to potable reuse. Environ. Sci. Technol. 51 (23), 13859-13868.
511 Crittenden, J.C., Hu, S., Hand, D.W., Green, S.A., 1999. A kinetic model for H_2O_2/UV process in
512 a completely mixed batch reactor. Water Res. 33 (10), 2315-2328.
513 Duan, X., Sanan, T., de la Cruz, A., He, X., Kong, M., Dionysiou, D.D., 2018a. Susceptibility of
514 the algal toxin microcystin-LR to UV/chlorine process: Comparison with chlorination. Environ.
515 Sci. Technol. 52 (15), 8252-8262.
516 Duan, X., Sun, H., Shao, Z., Wang, S., 2018b. Nonradical reactions in environmental remediation
517 processes: Uncertainty and challenges. Appl. Catal. B-Environ. 224, 973-982.
518 Duesterberg, C.K., Waite, T.D., 2006. Process optimization of Fenton oxidation using kinetic
519 modeling. Environ. Sci. Technol. 40 (13), 4189-4195.
520 Duesterberg, C.K., Waite, T.D., 2007. Kinetic modeling of the oxidation of p-hydroxybenzoic acid
521 by Fenton's reagent: Implications of the role of quinones in the redox cycling of iron. Environ.
522 Sci. Technol. 41 (11), 4103-4110.
523 Fang, C., Xiao, D., Liu, W., Lou, X., Zhou, J., Wang, Z., Liu, J., 2016. Enhanced AOX
524 accumulation and aquatic toxicity during 2,4,6-trichlorophenol degradation in a
525 Co(II)/peroxymonosulfate/Cl(-) system. Chemosphere 144, 2415-2420.

526 Grebel, J.E., Pignatello, J.J., Mitch, W.A., 2010. Effect of halide ions and carbonates on organic
527 contaminant degradation by hydroxyl radical-based Advanced Oxidation Processes in saline
528 waters. Environ. Sci. Technol. 44 (17), 6822-6828.
529 Guo, X., Minakata, D., Crittenden, J., 2014a. Computer-based first-principles kinetic Monte Carlo
530 simulation of polyethylene glycol degradation in aqueous phase UV/H_2O_2 advanced oxidation
531 process. Environ. Sci. Technol. 48 (18), 10813-10820.
532 Guo, X., Minakata, D., Niu, J., Crittenden, J., 2014b. Computer-based first-principles kinetic
533 modeling of degradation pathways and byproduct fates in aqueous-phase advanced oxidation
534 processes. Environ. Sci. Technol. 48 (10), 5718-5725.
535 Held, A.M., Halko, D.J., Hurst, J.K., 1978. Mechanisms of chlorine oxidation of hydrogen
536 peroxide. J. Am. Chem. Soc. 100 (18), 5732-5740.
537 Huang, K.Z., Zhang, H., 2019. Direct electron-transfer-based peroxymonosulfate activation by
538 iron-doped manganese oxide (δ-MnO_2) and the development of Galvanic Oxidation Processes
539 (GOPs). Environ. Sci. Technol. 53 (21), 12610-12620.
540 Huang, K.Z., Zhang, H., 2020a. Galvanic oxidation processes (GOPs): An effective direct electron
541 transfer approach for organic contaminant oxidation. Sci. Total Environ. 743, 140828.
542 Huang, K.Z., Zhang, H., 2020b. Highly efficient bromide removal from shale gas produced water
543 by unactivated peroxymonosulfate for controlling disinfection byproduct formation in impacted
544 water supplies. Environ. Sci. Technol. 54 (8), 5186-5196.
545 Ianni, J.C., Kintecus, Windows version 6.8, 2019. www.kintecus.com.
546 Kamath, D., Mezyk, S.P., Minakata, D., 2018. Elucidating the elementary reaction pathways and
547 kinetics of hydroxyl radical-induced acetone degradation in aqueous phase advanced oxidation
548 processes. Environ. Sci. Technol. 52 (14), 7763-7774.

549 Kang, N., Lee, D.S., Yoon, J., 2002. Kinetic modeling of Fenton oxidation of phenol and
550 monochlorophenols. Chemosphere 47 (9), 915-924.
551 Khan, A.U., Kasha, M., 1970. Chemiluminescence arising from simultaneous transitions in pairs
552 of singlet oxygen molecules. J. Am. Chem. Soc. 92 (11), 3293-3300.
553 Kong, X., Wu, Z., Ren, Z., Guo, K., Hou, S., Hua, Z., Li, X., Fang, J., 2018. Degradation of lipid
554 regulators by the UV/chlorine process: Radical mechanisms, chlorine oxide radical (ClO(*))-
555 mediated transformation pathways and toxicity changes. Water Res. 137, 242-250.
556 Lee, J., von Gunten, U., Kim, J.H., 2020. Persulfate-based advanced oxidation: Critical assessment
557 of opportunities and roadblocks. Environ. Sci. Technol. 54 (6), 3064-3081.
558 Li, K., Stefan, M.I., Crittenden, J.C., 2004. UV photolysis of trichloroethylene: Product study and
559 kinetic modeling. Environ. Sci. Technol. 38 (24), 6685-6693.
560 Li, K., Stefan, M.I., Crittenden, J.C., 2007. Trichloroethene degradation by UV/H_2O_2 advanced
561 oxidation process: product study and kinetic modeling. Environ. Sci. Technol. 41 (5), 1696-1703.
562 Li, X., Liu, J., Rykov, A.I., Han, H., Jin, C., Liu, X., Wang, J., 2015. Excellent photo-Fenton
563 catalysts of Fe–Co Prussian blue analogues and their reaction mechanism study. Appl. Catal. B-
564 Environ. 179, 196-205.
565 Lin, J.-M., Liu, M., 2008. Chemiluminescence from the decomposition of peroxymonocarbonate
566 catalyzed by gold nanoparticles. J. Phys. Chem. B 112 (26), 7850-7855.
567 Liu, M., Zhao, L., Lin, J.-M., 2006. Chemiluminescence energy transfer reaction for the on-line
568 preparation of peroxymonocarbonate and Eu(II)−dipicolinate complex. J. Phys. Chem. A 110 (23),
569 7509-7514.

570 Luo, C., Sadhasivan, M., Kim, J., Sharma, V.K., Huang, C.H., 2021. Revelation of Fe(V)/Fe(IV)
571 Involvement in the Fe(VI)-ABTS System: Kinetic Modeling and Product Analysis. Environ. Sci.
572 Technol. 55 (6), 3976-3987.
573 Luo, R., Li, M., Wang, C., Zhang, M., Nasir Khan, M.A., Sun, X., Shen, J., Han, W., Wang, L.,
574 Li, J., 2019. Singlet oxygen-dominated non-radical oxidation process for efficient degradation of
575 bisphenol A under high salinity condition. Water Res. 148, 416-424.
576 Monteagudo, J.M., Durán, A., González, R., Expósito, A.J., 2015. In situ chemical oxidation of
577 carbamazepine solutions using persulfate simultaneously activated by heat energy, UV light, Fe^{2+}
578 ions, and H_2O_2. Appl. Catal. B-Environ. 176-177, 120-129.
579 Mora, V.C., Rosso, J.A., Martire, D.O., Gonzalez, M.C., 2011. Phenol depletion by thermally
580 activated peroxydisulfate at 70 degrees C. Chemosphere 84 (9), 1270-1275.
581 Olmez-Hanci, T., Arslan-Alaton, I., 2013. Comparison of sulfate and hydroxyl radical based
582 advanced oxidation of phenol. Chem. Eng. J. 224, 10-16.
583 Pavitt, A.S., Bylaska, E.J., Tratnyek, P.G., 2017. Oxidation potentials of phenols and anilines:
584 correlation analysis of electrochemical and theoretical values. Environ. Sci.: Process. Impacts 19
585 (3), 339-349.
586 Piatt, J., O'brien, P.J., 1979. Singlet oxygen formation by a peroxidase, H_2O_2 and halide system.
587 Eur. J. Biochem. 93 (2), 323-332.
588 Qi, C., Liu, X., Ma, J., Lin, C., Li, X., Zhang, H., 2016. Activation of peroxymonosulfate by base:
589 Implications for the degradation of organic pollutants. Chemosphere 151, 280-288.
590 Qian, Y., Guo, X., Zhang, Y., Peng, Y., Sun, P., Huang, C.H., Niu, J., Zhou, X., Crittenden, J.C.,
591 2016. Perfluorooctanoic acid degradation using UV-persulfate process: Modeling of the
592 degradation and chlorate formation. Environ. Sci. Technol. 50 (2), 772-781.

593 Stanbury, D.M., 2020. Mechanisms of advanced oxidation processes, the principle of detailed
594 balancing, and specifics of the UV/chloramine process. Environ. Sci. Technol. 54 (7), 4658-4663.
595 Stanbury, D.M., Harshman, J., 2019. Large-scale models of radiation chemistry and the principle
596 of detailed balancing. J. Phys. Chem. A 123 (47), 10240-10245.
597 Wang, J., Wang, S., 2018. Activation of persulfate (PS) and peroxymonosulfate (PMS) and
598 application for the degradation of emerging contaminants. Chem. Eng. J. 334, 1502-1517.
599 Wang, Z., Feng, M., Fang, C., Huang, Y., Ai, L., Yang, F., Xue, Y., Liu, W., Liu, J., 2017. Both
600 degradation and AOX accumulation are significantly enhanced in UV/peroxymonosulfate/4-
601 chlorophenol/Cl− system: two sides of the same coin? RSC Adv. 7 (20), 12318-12321.
602 Wu, Z., Fang, J., Xiang, Y., Shang, C., Li, X., Meng, F., Yang, X., 2016. Roles of reactive chlorine
603 species in trimethoprim degradation in the UV/chlorine process: Kinetics and transformation
604 pathways. Water Res. 104, 272-282.
605 Yang, F., Sheng, B., Wang, Z., Yuan, R., Xue, Y., Wang, X., Liu, Q., Liu, J., 2019. An often-
606 overestimated adverse effect of halides in heat/persulfate-based degradation of wastewater
607 contaminants. Environ. Int. 130, 104918.
608 Yang, Y., Pignatello, J.J., Ma, J., Mitch, W.A., 2014. Comparison of halide impacts on the
609 efficiency of contaminant degradation by sulfate and hydroxyl radical-based advanced oxidation
610 processes (AOPs). Environ. Sci. Technol. 48 (4), 2344-2351.
611 Yang, Y., Pignatello, J.J., Ma, J., Mitch, W.A., 2016. Effect of matrix components on UV/H_2O_2
612 and UV/$S_2O_8^{(2-)}$ advanced oxidation processes for trace organic degradation in reverse osmosis
613 brines from municipal wastewater reuse facilities. Water Res. 89, 192-200.
614 Zagal, J.H., Ponce, I., Oñate, R., 2019. Redox, IntechOpen.

615 Zhang, K., Parker, K.M., 2018. Halogen radical oxidants in natural and engineered aquatic systems.
616 Environ. Sci. Technol. 52 (17), 9579-9594.
617 Zhang, R., Sun, P., Boyer, T.H., Zhao, L., Huang, C.H., 2015. Degradation of pharmaceuticals and
618 metabolite in synthetic human urine by UV, UV/H_2O_2, and UV/PDS. Environ. Sci. Technol. 49
619 (5), 3056-3066.
620 Zhao, X., Li, Y., Lu, J., Zhou, L., Chovelon, J.-M., Zhou, Q., Ji, Y., 2021. UV/H_2O_2 oxidation of
621 chloronitrobenzenes in waters revisited: Hydroxyl radical induced self-nitration. J. Photochem.
622 Photobiol. A: Chem. 410.
623 Zhong, S., Hu, J., Fan, X., Yu, X., Zhang, H., 2020a. A deep neural network combined with
624 molecular fingerprints (DNN-MF) to develop predictive models for hydroxyl radical rate constants
625 of water contaminants. J. Hazard. Mater. 383, 121141.
626 Zhong, S., Zhang, K., Wang, D., Zhang, H., 2020b. Shedding Light On “Black Box” Machine
627 Learning Models for Predicting the Reactivity of HO• Radicals toward Organic Compounds.
628 Chem. Eng. J., 126627.
629 Zhou, L., Song, W., Chen, Z., Yin, G., 2013. Degradation of organic pollutants in wastewater by
630 bicarbonate-activated hydrogen peroxide with a supported cobalt catalyst. Environ. Sci. Technol.
631 47 (8), 3833-3839.
632 Zhou, Y., Jiang, J., Gao, Y., Pang, S.Y., Ma, J., Duan, J., Guo, Q., Li, J., Yang, Y., 2018. Oxidation
633 of steroid estrogens by peroxymonosulfate (PMS) and effect of bromide and chloride ions:
634 Kinetics, products, and modeling. Water Res. 138, 56-66.

635